Twisted light transmission over 143 km

Mario Krenn[a,b,1], Johannes Handsteiner[a,b], Matthias Fink[b], Robert Fickler[a,b,c,d], Rupert Ursin[b], Mehul Malik[a,b], and Anton Zeilinger[a,b,1]

[a]Faculty of Physics, Vienna Center for Quantum Science and Technology, University of Vienna, A-1090 Vienna, Austria; [b]Institute for Quantum Optics and Quantum Information, Austrian Academy of Sciences, A-1090 Vienna, Austria; [c]Department of Physics, University of Ottawa, Ottawa, ON, Canada K1N 6N5; and [d]Max Planck Centre for Extreme and Quantum Photonics, University of Ottawa, Ottawa, ON, Canada K1N 6N5

Contributed by Anton Zeilinger, October 13, 2016 (sent for review June 9, 2016; reviewed by Andrew Forbes, Jonathan Leach, and Bo Thidé)

Spatial modes of light can potentially carry a vast amount of information, making them promising candidates for both classical and quantum communication. However, the distribution of such modes over large distances remains difficult. Intermodal coupling complicates their use with common fibers, whereas free-space transmission is thought to be strongly influenced by atmospheric turbulence. Here, we show the transmission of orbital angular momentum modes of light over a distance of 143 km between two Canary Islands, which is 50× greater than the maximum distance achieved previously. As a demonstration of the transmission quality, we use superpositions of these modes to encode a short message. At the receiver, an artificial neural network is used for distinguishing between the different twisted light superpositions. The algorithm is able to identify different mode superpositions with an accuracy of more than 80% up to the third mode order and decode the transmitted message with an error rate of 8.33%. Using our data, we estimate that the distribution of orbital angular momentum entanglement over more than 100 km of free space is feasible. Moreover, the quality of our free-space link can be further improved by the use of state-of-the-art adaptive optics systems.

high-dimensional states | long-distance communication | orbital angular momentum | atmospheric turbulence

The transverse spatial modes of light offer an additional degree of freedom for encoding information in both classical and quantum communication. In classical communication, such modes can be used for multiplexing information and for increasing the achievable data rate per frequency and polarization channel (1–4); for recent reviews, see refs. 5 and 6. In quantum information science they are a physical realization of a high-dimensional quantum state (7–12). Such states allow one to encode more than 1 bit of information per photon. The large state space can increase the channel capacity and improve robustness to eavesdropping and noise (13, 14) in quantum communication schemes (15–18). The distribution of photons carrying different spatial modes over macroscopic distances is thus essential for both quantum and classical applications, as well as for fundamental tests of quantum mechanics. Whereas significant progress has been made in fiber-based solutions (19, 20), these methods are still in their infancy. Here we focus on a different way to distribute such modes, namely long-distance transmission through free space. This is relevant in situations where fibers are not applicable, such as for long-distance quantum communication and communication with satellites.

Atmospheric turbulence plays a significant role in the free-space transmission of spatial modes. These effects of the atmosphere have been investigated in many recent theoretical studies (21–27) and laboratory-scale simulations (28–33). Although these investigations clearly show that transmitting spatial modes of light over large distances is very challenging, recently several experimental investigations of free-space long-distance transmission of spatial modes have been successfully carried out. Most of them use so-called "twisted light modes," where the phase front of the light has a helical or twisted phase structure. As these modes can carry an integer number of orbital angular momentum (OAM) quanta, they are often referred to as OAM modes. In 2012, a classical communication experiment with twisted radio waves was performed over ∼420 m in Venice, Italy (34). Single photons carrying OAM in the visible frequency were transmitted over ∼210 m in a quantum key distribution experiment in Padua, Italy (35). The experiment was carried out inside a large hall, as light in the visible frequency is significantly more influenced by the turbulence because of shorter wavelengths. More recently, 16 different spatial modes were used to encode information for classical communication over an intracity 3-km link across Vienna (36). In the same 3-km link, quantum entanglement encoded in the OAM degree of freedom was transmitted using the first two higher-order OAM modes (37), demonstrating that single-photon spatial coherence and two-photon coherence of spatial modes survive in a turbulent long-distance link. One experiment in Erlangen, Germany tested classical transmission and cross-talk of OAM beams over 1.6 km (38). Finally, a high-speed classical communication experiment using OAM mode multiplexing was performed over 120 m of free space in Los Angeles, transmitting 400 GBit/s (39).

In this work, we test the effect of atmospheric turbulence on a 143-km OAM free-space link between two Canary Islands, La Palma and Tenerife. In doing so, our experiment increases the maximum distance achieved in a free-space OAM link by a factor of 50. We use OAM mode superpositions of $\ell = \pm 1$, ± 2, and ± 3 with different relative phases for encoding information. The relative phases result in a rotation of the mode structure, which allows these modes to be distinguished according to their intensity. This technique has previously been exploited to investigate the transmission quality in both a classical (36) and a quantum experiment (37) in an intracity 3-km link. For characterization of the received mode quality, we record images of the intensity

Significance

Light is the main carrier of information. Its spatial mode allows the encoding of more than 1 bit per photon, and thus can increase the information capacity. For communication purposes, these modes need to be transmitted over large distances. Nowadays, fiber-based solutions are in their infancy, which renders free-space transmission the only possibility. We present an experiment where we investigate the behavior of the spatial modes after a distance of 143 km. With the help of an artificial neural network, we distinguished different mode superpositions up to the third order with more than 80% accuracy. Our results indicate that with state-of-the-art adaptive optics systems, both classical communication and entanglement transmission is feasible over distances of more than 100 km.

Author contributions: M.K., J.H., M.F., R.F., R.U., M.M., and A.Z. designed research; M.K., J.H., M.F., R.F., and M.M. performed research; M.K. analyzed data; A.Z. conceived and supervised the research; and M.K., J.H., M.F., R.F., R.U., M.M., and A.Z. wrote the paper.

Reviewers: A.F., University of the Witwatersrand; J.L., Heriot-Watt University; and B.T., Swedish Institute of Space Physics.

The authors declare no conflict of interest.

[1]To whom correspondence may be addressed. Email: mario.krenn@univie.ac.at or anton.zeilinger@univie.ac.at.

This article contains supporting information online at www.pnas.org/lookup/suppl/doi:10.1073/pnas.1612023113/-/DCSupplemental.

distribution observed on the white wall of the telescope *Observatorio del Teide* and analyze them with a pattern recognition algorithm based on an artificial neural network. By calculating the cross-talk, we find that the modal structure can be distinguished quite well even without the use of any adaptive optics correcting for the effects of atmospheric turbulence. Finally, to visualize the quality of the transmission, we use these modes to encode, transmit, and recover a short message.

In the experiment, we use the paraxial approximation of the full electromagnetic field, which leads to scalar solutions for light beams. For a more rigorous treatment of spatial modes with exact representations of the complete electromagnetic vector fields, see ref. 6. A solution to the paraxial wave equation defines the transverse structure of the light beam, and those orthogonal modes we call (transverse) spatial modes. The solution we work with are Laguerre–Gauss (LG) modes of light, which are characterized by a spiral phase distribution $\exp(i\ell\varphi)$, where the mode number ℓ can only take integer values and stands for the orbital angular momentum or topological charge of the photons (40). The radial mode number is zero in all experiments. In the center of the beam, a phase singularity leads to an intensity null along the beam axis, which gives OAM modes a ring-shaped intensity pattern. Equally weighted superpositions of LG modes with opposite OAM can be written as

$$LG^{\alpha}_{\pm\ell}(r,\varphi) = \frac{1}{\sqrt{2}}\left(LG_{+\ell}(r,\varphi) + e^{i\alpha}LG_{-\ell}(r,\varphi)\right),$$

where α denotes the relative phase between the two modes. The transverse phase is radially uniform and has 2ℓ phase jumps of π in the azimuthal direction, which leads to 2ℓ maxima and minima arranged symmetrically in a ring. The phase α is directly related to the angular position of the structure $\gamma = (360°/2\pi)(\alpha/2\ell)$. Hence, a simple determination of the angular position, e.g., by recording the intensity structure, can be used to reveal the relative phase in classical (36) and even in quantum experiments (37, 41, 42).

A schematic of the experimental setup for sending and receiving the spatial modes can be seen in Fig. 1*A*. At the sending station on the island of La Palma, a green laser with a wavelength of 532 nm and a power of 60 mW was used for encoding the twisted light modes and their superpositions. The laser was modulated with a phase-only spatial light modulator (SLM), which imprinted the spatial modes on the beam with holograms without amplitude modulation. Phase-only holograms, as used by us, produce vortex beams with a slightly different radial structure compared with LG modes. This difference is not relevant in our experiment. Then, the beam was magnified with a telescope to ∼4-cm diameter, and transmitted with a high-quality f = 28 cm lens through 143 km of free space to the island of Tenerife, where the receiver was located. In vacuum, the beam diameter would be expected to be roughly 1.3 m, whereas we observe significantly larger beams due to beam spreading introduced by the atmosphere. At the receiver in Tenerife, the mode structure was observed on the white wall of an observatory (with a diameter of roughly 11 m) and recorded with a Nikon D3S camera with varying exposure times. A beacon laser shining back from Tenerife to La Palma was used for initial alignment. However, no active tracking or adaptive optics was used to correct the atmospheric turbulence during the data transmission itself. The recorded images were then analyzed to recover the encoded information in an automatized manner.

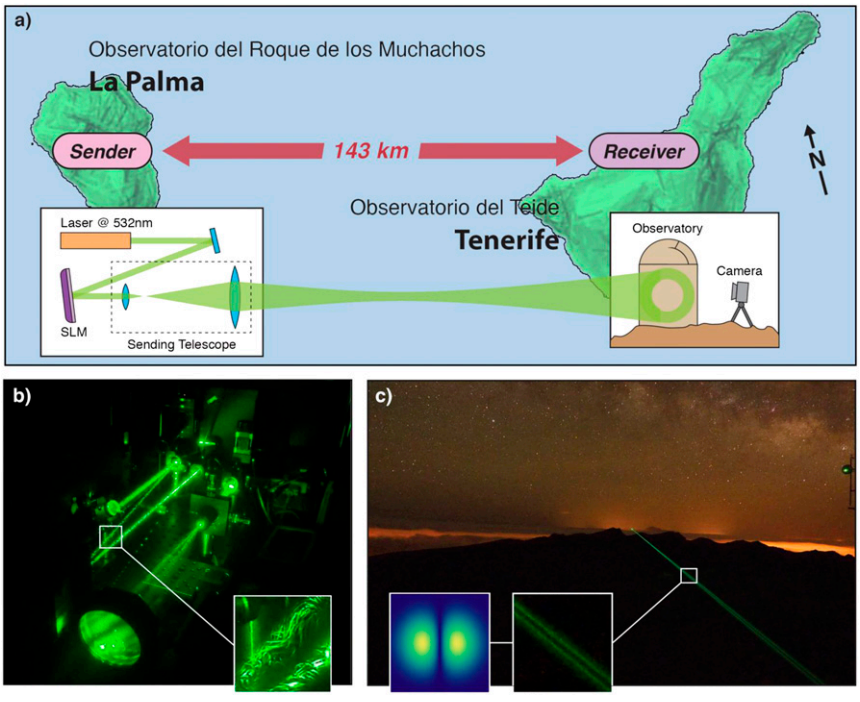

Fig. 1. (*A*) Sketch of the experimental setup. The sender is located on the roof of the Jacobus Kapteyn telescope on the island of La Palma and consists of a 60-mW laser with a wavelength of 532 nm modulated by an SLM. Different phase holograms on the SLM encode different spatial modes. The modes are magnified with a sending telescope and sent over 143 km to the receiver at the island of Tenerife. Extra mirrors used in the actual sending setup are not shown for simplicity. The structure of received modes is observed on the wall of the Optical Ground Station telescope owned by the ESA and recorded with a camera. (*B*) Photo of the sender taken during extremely turbulent conditions on La Palma. (*Inset*) Small vortices and eddies formed by the water vapor in the air are clearly visible. At the sending lens an $\ell = \pm 1$ can be seen. Modes sent under these conditions were not discernible at the receiver. (*C*) Long-time exposure photo showing an OAM superposition of $\ell = \pm 1$ being transmitted over the Caldera de Taburiente (silhouetted in black) from La Palma to Tenerife. (*Insets*) Note that the double-lobed modal structure of the beam is clearly visible. A theoretical plot of the mode superposition cross-section is shown for comparison.

Fig. 1*B* shows the sending setup in very strong turbulence conditions on La Palma. Vortices and eddies formed by water vapor droplets in the air can be clearly seen in Fig. 1*B* (*Inset*). We were unable to recognize any spatial modes transmitted during such atmospheric conditions. The long-time exposure photograph in Fig. 1*C* was taken under much better atmospheric conditions and shows an $\ell = \pm 1$ superposition being transmitted from La Palma to Tenerife, over the edge of the crater wall of the Caldera de Taburiente. The insets show that the double-lobed structure of the mode is clearly visible in the transmitted beam.

To characterize the turbulence, we took long-time exposure photographs of a Gaussian beam shining back from the receiver toward the sender at La Palma and investigated the observed beam spread. Without atmosphere one would expect a point-spread function (PSF) with an FWHM = λ/D, where D is the effective aperture of the objective. Propagation through turbulent media enlarges the diameter of the PSF, which leads to an $\mathrm{FWHM_{obs}}$, and can be characterized by the Fried parameter r0 that is defined by $\mathrm{r0} = \lambda/\mathrm{FWHM_{obs}}$. We used an Olympus E-M10 camera and an objective with an f-stop of f/5.6 and focal length f = 200 mm to record images of the tracking beam at La Palma. The effective aperture of this system was D = 35 mm and therefore twice as big as the expected r0. During the observation period, the Fried parameter varied between 0.4 and 1.3 cm, which is consistent with measurements over the same link from earlier years (43) and is considered to demonstrate strong turbulence.

We performed the measurements over 10 successive nights. On four of these nights we analyzed data for mode superpositions, and on two nights we recorded pure vortex modes. On the remaining four nights the weather conditions were too bad to recognize any mode structure. This was either because of fog or clouds between the two islands that significantly reduced the received laser intensity, or because of the presence of strong turbulence that significantly deteriorated the mode quality. In these cases, the Fried parameter r0 of the link was below 1 cm. For more details, see Table S2.

When the Fried parameter r0 was above 1 cm, we were able to discern the OAM modes received at Tenerife. Examples of four such OAM mode superpositions as well as four pure vortex modes are shown in Fig. 2. The lobed modal structure is clearly visible for modes with $\ell = \pm 1$, ± 2, and ± 3 in Fig. 2 *A–D*. The relative phase of π introduced in the $\ell = \pm 3$ mode superposition is clearly seen to rotate the mode structure by an angle of $\pi/3$ in Fig. 2 *C* and *D*. Examples of four different pure vortex modes (ℓ = 3, 4, 5, and 7) received after 143 km are shown in Fig. 2 *E–H*. As expected, the mode diameter gets larger as the OAM quantum number ℓ is increased, and is seen to approach the size of the telescope wall for $\ell = 7$.

In the next step, we estimate the quality of the transmission. We are only interested in the quality of the relative phase of LG superpositions; thus, a full mode decomposition (which would require the complete complex mode) is not required. The advantage of our method is that the relative phase of LG superpositions is visible directly from intensity measurements, thus allowing us to estimate their quality in the transmission from the recoded images alone. The mapping of observed intensities to the relative-phase information was done with a pattern recognition algorithm which, for every image, returns the most likely relative phase (see *Supporting Information* and Table S1 for more details).

The algorithm is based on an artificial unsupervised neural network, also known as a self-organizing feature map (44, 45). The idea, which has been used and explained in detail in ref. 36, is to supply the neural network with a training set of images. The images are then characterized automatically according to their respective features. After this training phase, the network can analyze real data in the form of images. The training set consists of images that were sent through the same turbulent link, allowing the algorithm to automatically find a robust characterization of images of modes exposed to turbulence.

Using this detection method, we are able to calculate crosstalk matrices between the sent and received modes. The crosstalk matrix shows to what quality the neural network was able to correctly identify the received image (more details in *Supporting Information*). We analyze superposition structures and their angular rotations, which correspond to different relative phases $\Delta\alpha$ between the modes (Fig. 3, *Upper*). For $\ell = \pm 1$ we accumulate 250 images with 8 different relative phases of $\Delta\alpha = \pi/4$, which correspond to 8 different spatial orientations. Forty of those images (five per orientation) are used for training of the neural network. After the training phase, the remaining 210 images are analyzed by the network one after another. Comparing the input and the output of the neural network, we find that nearly 80%

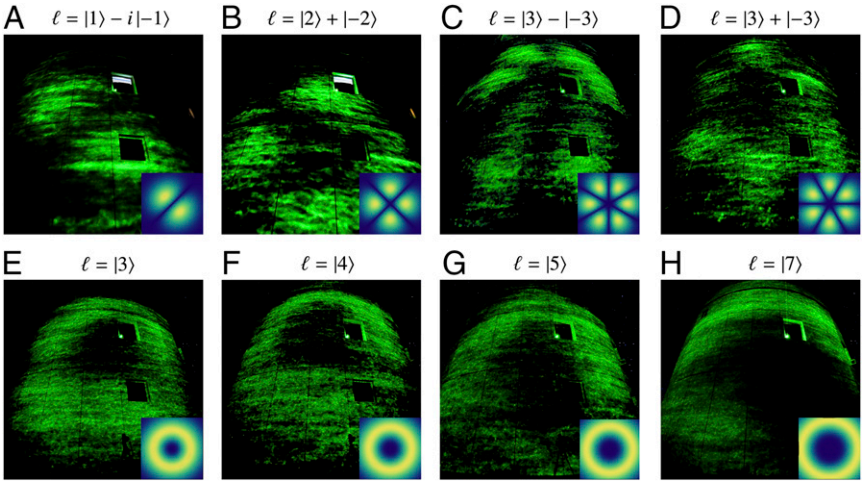

Fig. 2. (*A–D*) Examples of OAM mode superpositions received on the wall of the telescope *Observatorio del Teide* after propagating through 143 km of free space between the islands of La Palma and Tenerife. The diameter of the observatory is roughly 11 m. The lobed modal structure is clearly visible for mode superpositions with $\ell = \pm 1$, ± 2, and ± 3. Images *C* and *D* show the rotation of an $\ell = \pm 3$ mode superposition by $\pi/3$ when the relative phase α is changed by π. (*E–H*) Examples of pure OAM (vortex) modes observed at the receiver. The intensity null at the center of the modes is clearly visible. The mode diameter gets larger as the OAM quantum number ℓ is increased, and is seen to approach the size of the telescope wall for $\ell = 7$. The size of the modes clearly increases for higher orders. Note that these images were taken at a time when atmospheric conditions were stable.

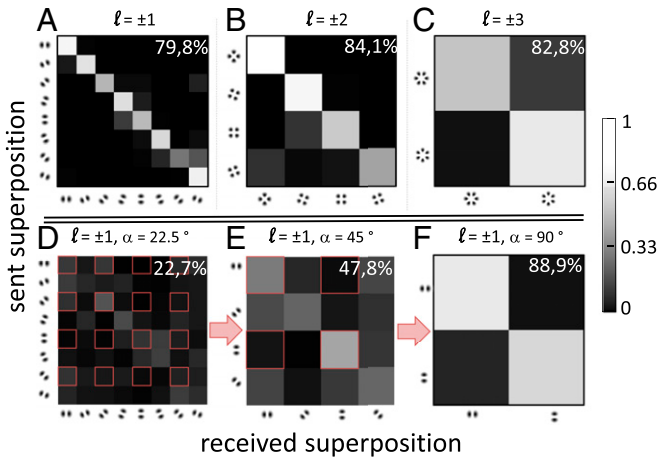

Fig. 3. Cross-talk matrices showing the success probability with which the transmitted OAM mode superpositions were correctly identified at the receiver. (*A*–*C*) Results for superpositions of $\ell = \pm 1$, ± 2, and ± 3 modes with relative phases of $\Delta\alpha = \pi/4$, $\pi/2$, and π, respectively. The different relative phases correspond to different rotations of the superposition structure. The received modes were correctly identified by our detection algorithm with an average success probability of 82%. (*D*) During a turbulent night, eight modes consisting of superpositions of $\ell = \pm 1$ were identified with a success probability of only 22.7%. When we restrict ourselves to a subset of these modes with $\Delta\alpha = \pi/2$ or π (highlighted with red squares and reanalyzed by the neural network each time), the success probability increases significantly (*E* and *F*). The ability to resolve all eight of these modes is required for device-independent quantum key distribution (violation of a Bell inequality), four modes are necessary for entanglement-based quantum key distribution (violation of an entanglement witness), and two modes can be used for classical communication with 1 bit per mode.

of the different rotation angles of the structure were correctly identified. For $\ell = \pm 2$ with four different settings of $\Delta\alpha = \pi/2$, 84% of the mode images were correctly identified. For superpositions made up of $\ell = \pm 3$, two different relative phases $\Delta\alpha = \pi/2$ were identified with nearly 83% certainty. From this, a channel capacity can be calculated of 2.24 bits, 1.45 bits, and 0.39 bits per shot, for $\ell = \pm 1$, ± 2, and ± 3, respectively. On certain nights, the atmospheric conditions did not allow small phase changes to be identified very well, as seen by the success rate of 22.7% for $\ell = \pm 1$ and $\Delta\alpha = \pi/4$ (Fig. 3*D*). By restricting ourselves to a smaller subset of these modes, we were able to increase the success rate to 47.8% and 88.9% for $\Delta\alpha = \pi/2$ and $\Delta\alpha = \pi$, respectively. Verifying the presence of OAM entanglement requires one to measure different mode superpositions with at least $\Delta\alpha = \pi/2$. This indicates that in certain conditions where quantum communication would break down, classical communication using OAM states might still be possible. By analyzing intensity images, we estimate the expected visibility in a quantum entanglement experiment to be ~60%, which indicates that the distribution of quantum entanglement over this link encoded in spatial modes is not prevented by atmospheric turbulence (see *Supporting Information* for more details).

As a final test of the transmission quality, we encoded a short message ("Hello World!") in modes $\ell = \pm 1$ with four different relative phases corresponding to $\Delta\alpha = \pi/2$ (Fig. 4). The message was encoded using a 64-letter alphabet with upper- and lowercase letters, as well as numbers, space, and exclamation mark. In this alphabet, every letter needs 6 bits of information for encoding. We encoded each letter by using three consecutively transmitted superposition modes, with each mode in one out of four phase settings. Thus, each mode carries 2 bits of information, which leads to $4^3 = 2^6 = 64$ settings. We recorded five 1-s-long exposures of every mode, resulting in a total of 180 images. Out of these, 72 images were chosen at random and used to train the neural network. The network then analyzed the remaining 108 images to decode the message. Each letter was redundantly encoded three times as a simple form of error correction. The network decoded the message as "Hello WorldP," where the last letter contains one (out of three) wrongly detected mode. The error per letter is 8.33% (1 out of 12 letters is wrong), the error per bit is 1.4% (1 out of 72 bits is wrong). The individual modes were identified correctly with a probability of 76.3%. The complete transmission (including delimiters) took 271 s, which corresponds to a speed comparable to that of smoke signaling—the first form of long-distance communication in ancient times (46), or to that of communication with neutrinos (47).

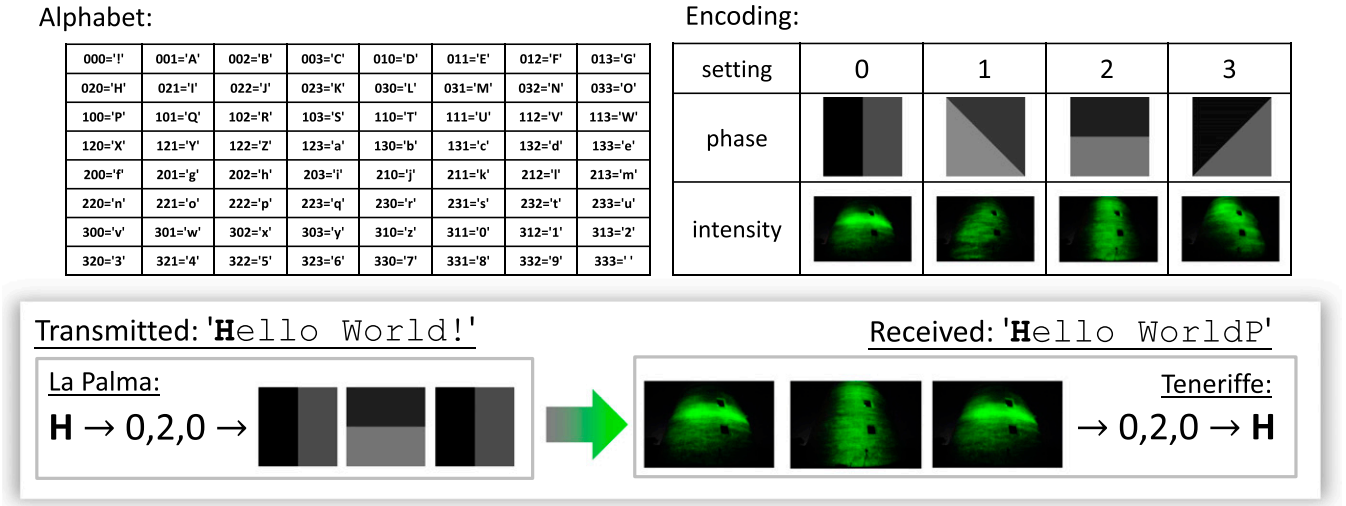

Fig. 4. Encoding and decoding of a short message with twisted light superpositions. The message "Hello World!" is sent letter by letter. Every letter is encoded into three $\ell = \pm 1$ superpositions with four different relative phase settings. For example, the letter "H" is encoded as 0, 2, and 0. Thus, every mode corresponds to 2 bits of information. After 143 km of transmission, the modes are recorded and characterized with an artificial neural network. The same alphabet is used to decode the letter from the mode superpositions. The final recorded message is "Hello WorldP." The last letter is a "P" (which is encoded as 1,0,0) instead of an "!" (which is encoded as 0,0,0). This error is due to one incorrectly detected mode.

The quality of the received OAM modes was primarily reduced due to turbulence near the sender—above the Taburiente caldera. The outgoing laser beam was shifted laterally by this turbulence, effectively smearing out the modes received at Tenerife. This first-order effect can be corrected to some extent by using a tip-tilt motor that relies on a beacon laser sent from Tenerife. The correction speed is limited by three primary factors: (*i*) the physical interisland distance of 143 km, which corresponds to a travel time of 0.5 ms; (*ii*) The processing speed of the computer running the correction software; and (*iii*) the tip-tilt motor speed and response time. To improve the mode quality in future experiments, one would need to address all three of these points. The physical distance limitation can be addressed by having a second beacon laser closer to the sender. One could illuminate the edge of the caldera wall with a laser beam, thus creating a second "guide star" closer to the sender. This would provide information exclusively about the local turbulence around the sender, which causes a stronger effect on the lateral movement of the received modes than turbulence around the receiver. The second point can be simply addressed by using a fast computer and modern turbulence-compensation software. Finally, a small, two-axis, piezo-controlled mirror placed just before the sending lens could provide fast tip-tilt correction. Taking all these improvements into account, we believe that the quality of the modes received after 143 km of propagation can be improved substantially in future experiments. Furthermore, with this increased pointing stability, performing quantum experiments with the OAM of photons should be feasible (37).

In conclusion, we have investigated the transmission of twisted light modes and their superpositions over a 143-km free-space link between the two Canary Islands, La Palma and Tenerife. Without any active compensation for the effects of turbulence, we find that the relative orientations of the first three higher-order mode superpositions can be distinguished with an average success probability of 82%. This indicates that the long-distance distribution of quantum entanglement of orbital angular momentum modes might be feasible in the future. To demonstrate the quality of the link, we transmitted and successfully decoded a short message encoded in the twisted light superpositions. We do not consider this method as real communication but merely the demonstration of the transmission quality of modes. However, the application of state-of-the-art adaptive optics such as those used in simple and efficient intensity-based methods (48) could further improve the link quality, potentially enabling its application in a multiplexing scheme for classical communication (39). Furthermore, the effective thickness of the atmosphere is 6 km (49), which is well below our link distance, indicating that earth-to-satellite communication with spatially encoded modes is not limited by atmospheric turbulence.

ACKNOWLEDGMENTS. We thank Zoran Sodnik from the European Space Agency (ESA) and J. Carlos from Instituto de Astrofísica de Canarias for support. This work was supported by the ESA, the Austrian Academy of Sciences, the Austrian Federal Ministry of Science, Research and Economy, the European Research Council (Simulators and Interfaces with Quantum Systems Grant 600645 EU-FP7-ICT), and the Austrian Science Fund with SFB F40 (Foundations and Applications of Quantum Science).

1. Gibson G, et al. (2004) Free-space information transfer using light beams carrying orbital angular momentum. *Opt Express* 12(22):5448–5456.
2. Wang J, et al. (2012) Terabit free-space data transmission employing orbital angular momentum multiplexing. *Nature Photonics* 6(7):488–496.
3. Huang H, et al. (2014) 100 Tbit/s free-space data link enabled by three-dimensional multiplexing of orbital angular momentum, polarization, and wavelength. *Opt Lett* 39(2):197–200.
4. Milione G, et al. (2015) 4 × 20 Gbit/s mode division multiplexing over free space using vector modes and a q-plate mode (de)multiplexer. *Opt Lett* 40(9):1980–1983.
5. Willner AE, et al. (2015) Optical communications using orbital angular momentum beams. *Adv Opt Photonics* 7(1):66–106.
6. Thidé B, Tamburini F, Then H, Someda CG, Ravanelli RA (2014) The physics of angular momentum radio. arXiv:1410.4268.
7. Vaziri A, Weihs G, Zeilinger A (2002) Experimental two-photon, three-dimensional entanglement for quantum communication. *Phys Rev Lett* 89(24):240401.
8. Agnew M, Leach J, McLaren M, Roux FS, Boyd RW (2011) Tomography of the quantum state of photons entangled in high dimensions. *Phys Rev A* 84(6):062101.
9. Dada AC, Leach J, Buller GS, Padgett MJ, Andersson E (2011) Experimental high-dimensional two-photon entanglement and violations of generalized Bell inequalities. *Nat Phys* 7(9):677–680.
10. Giovannini D, et al. (2013) Characterization of high-dimensional entangled systems via mutually unbiased measurements. *Phys Rev Lett* 110(14):143601.
11. Krenn M, et al. (2014) Generation and confirmation of a (100 x 100)-dimensional entangled quantum system. *Proc Natl Acad Sci USA* 111(17):6243–6247.
12. Malik M, Erhard M, Huber M, Krenn M, Fickler R, Zeilinger A (2016) Multi-photon entanglement in high dimensions. *Nat Photonics* 10(4):248–252.
13. Bourennane M, Karlsson A, Björk G (2001) Quantum key distribution using multilevel encoding. *Phys Rev A* 64(1):012306.
14. Huber M, Pawłowski M (2013) Weak randomness in device-independent quantum key distribution and the advantage of using high-dimensional entanglement. *Phys Rev A* 88(3):032309.
15. Gröblacher S, Jennewein T, Vaziri A, Weihs G, Zeilinger A (2006) Experimental quantum cryptography with qutrits. *New J Phys* 8(5):75.
16. Walborn SP, Lemelle DS, Almeida MP, Ribeiro PH (2006) Quantum key distribution with higher-order alphabets using spatially encoded qudits. *Phys Rev Lett* 96(9): 090501.
17. Mafu M, et al. (2013) Higher-dimensional orbital-angular-momentum-based quantum key distribution with mutually unbiased bases. *Phys Rev A* 88(3):032305.
18. Mirhosseini M, et al. (2015) High-dimensional quantum cryptography with twisted light. *New J Phys* 17(3):033033.
19. Bozinovic N, et al. (2013) Terabit-scale orbital angular momentum mode division multiplexing in fibers. *Science* 340(6140):1545–1548.
20. Ip E, et al. (2015) SDM transmission of real-time 10GbE traffic using commercial SFP + transceivers over 0.5km elliptical-core few-mode fiber. *Opt Express* 23(13):17120–17126.
21. Paterson C (2005) Atmospheric turbulence and orbital angular momentum of single photons for optical communication. *Phys Rev Lett* 94(15):153901.
22. Tyler GA, Boyd RW (2009) Influence of atmospheric turbulence on the propagation of quantum states of light carrying orbital angular momentum. *Opt Lett* 34(2):142–144.
23. Chandrasekaran N, Shapiro JH (2014) Photon information efficient communication through atmospheric turbulence–Part I: Channel model and propagation statistics. *J Lightwave Technol* 32(6):1075–1087.
24. Roux FS, Wellens T, Shatokhin VN (2015) Entanglement evolution of twisted photons in strong atmospheric turbulence. *Phys Rev A* 92(1):012326.
25. Avetisyan H, Monken CH (2016) Higher order correlation beams in atmosphere under strong turbulence conditions. *Opt Express* 24(3):2318–2335.
26. Chen C, Yang H, Tong S, Lou Y (2016) Changes in orbital-angular-momentum modes of a propagated vortex Gaussian beam through weak-to-strong atmospheric turbulence. *Opt Express* 24(7):6959–6975.
27. Leonhard ND, Shatokhin VN, Buchleitner A (2015) Universal entanglement decay of photonic-orbital-angular-momentum qubit states in atmospheric turbulence. *Phys Rev A* 91(1):012345.
28. Pors BJ, Monken CH, Eliel ER, Woerdman JP (2011) Transport of orbital-angular-momentum entanglement through a turbulent atmosphere. *Opt Express* 19(7):6671–6683.
29. Malik M, et al. (2012) Influence of atmospheric turbulence on optical communications using orbital angular momentum for encoding. *Opt Express* 20(12):13195–13200.
30. Ibrahim AH, Roux FS, McLaren M, Konrad T, Forbes A (2013) Orbital-angular-momentum entanglement in turbulence. *Phys Rev A* 88(1):012312.
31. Ren Y, et al. (2013) Atmospheric turbulence effects on the performance of a free space optical link employing orbital angular momentum multiplexing. *Opt Lett* 38(20):4062–4065.
32. Rodenburg B, et al. (2014) Simulating thick atmospheric turbulence in the lab with application to orbital angular momentum communication. *New J Phys* 16(3):033020.
33. Xie G, et al. (2015) Performance metrics and design considerations for a free-space optical orbital-angular-momentum–multiplexed communication link. *Optica* 2(4):357–365.
34. Tamburini F, et al. (2012) Encoding many channels on the same frequency through radio vorticity: First experimental test. *New J Phys* 14(3):033001.
35. Vallone G, et al. (2014) Free-space quantum key distribution by rotation-invariant twisted photons. *Phys Rev Lett* 113(6):060503.
36. Krenn M, et al. (2014) Communication with spatially modulated light through turbulent air across Vienna. *New J Phys* 16(11):113028.
37. Krenn M, Handsteiner J, Fink M, Fickler R, Zeilinger A (2015) Twisted photon entanglement through turbulent air across Vienna. *Proc Natl Acad Sci USA* 112(46): 14197–14201.
38. Lavery MP, et al. (2015) *Study of Turbulence Induced Orbital Angular Momentum Channel Crosstalk in a 1.6 km Free-Space Optical Link. CLEO: Science and Innovations* (Optical Society of America, Washington, DC), pp STu1L–4.
39. Ren Y, et al. (2016) Experimental characterization of a 400 Gbit/s orbital angular momentum multiplexed free-space optical link over 120 m. *Opt Lett* 41(3):622–625.
40. Allen L, Beijersbergen MW, Spreeuw RJC, Woerdman JP (1992) Orbital angular momentum of light and the transformation of Laguerre-Gaussian laser modes. *Phys Rev A* 45(11):8185–8189.
41. Fickler R, et al. (2012) Quantum entanglement of high angular momenta. *Science* 338(6107):640–643.
42. Fickler R, Krenn M, Lapkiewicz R, Ramelow S, Zeilinger A (2013) Real-time imaging of quantum entanglement. *Sci Rep* 3:1914.

43. Ursin R, et al. (2007) Entanglement-based quantum communication over 144 km. *Nat Phys* 3(7):481–486.
44. Kohonen T (1982) Self-organized formation of topologically correct feature maps. *Biol Cybern* 43(1):59–69.
45. Kohonen T (2001) *Self-Organizing Maps* (Springer, Berlin), Vol 30.
46. Brückner V (2013) *Optische Nachrichtentechnik: Grundlagen und Anwendungen* (Springer, Berlin). German.
47. Stancil DD, et al. (2012) Demonstration of communication using neutrinos. *Mod Phys Lett A* 27(12):1250077.
48. Xie G, et al. (2015) Phase correction for a distorted orbital angular momentum beam using a Zernike polynomials-based stochastic-parallel-gradient-descent algorithm. *Opt Lett* 40(7):1197–1200.
49. Bohren CF, Albrecht BA (1988) *Atmospheric Thermodynamics* (Oxford Univ Press, New York).